Article:
Lin, L-S, Bin-Tay, W, Li, Y-R et al. (3 more authors) (2020) A practical characterisation protocol for liquid-phase synthesised heterogeneous graphene. Carbon, 167. pp. 307-321. ISSN 0008-6223

https://doi.org/10.1016/j.carbon.2020.06.008

A practical characterisation protocol for liquid-phase synthesised heterogeneous graphene

Li-Shang Lin[1,2], Wei Bin-Tay[1], Yi-Ru Li[2,3], Zabeada Aslam[1], Aidan Westwood[*,1] and Rik Brydson[1]

[1]School of Chemical and Process Engineering, University of Leeds, Leeds LS2 9JT, UK

[2]Research Center of Applied Science (RCAS), Academia Sinica, Taipei, Taiwan

[3]Institute of Photonics and Optoelectronics, and Department of Electrical Engineering, National Taiwan University, Taipei, Taiwan

Abstract

We demonstrate a characterisation protocol for quantifying nanostructural features associated with heterogeneous graphene nanosheets, including the lateral dimension, thickness and defect density of flakes produced by liquid phase exfoliation methods. The underlying basis for the protocol is a cross correlation between high resolution electron probe-based techniques and lower resolution but higher throughput photon probe-based characterisation methods. Using statistical data analysis we are able to develop a practical characterisation protocol that provides access to the precision and accuracy of the various graphene characterisation techniques. We have shown that the lateral dimension and thickness of heterogeneous graphene flakes can be rapidly quantified via optical mapping techniques. The defect densities within graphene samples can be accessed via Raman micro-spectroscopy. Based on the high throughput photon probe-based characterisation method, statistically representative data for heterogeneous graphene nanosheets can be obtained. Such information can be used to differentiate between inhomogeneous graphene samples in large length scales and thus can be useful for optimising graphene synthesis processes.

1. Introduction

Graphene has received enormous attention due to its wide-ranging potential applications for

[*] Corresponding author. Tel: +44 113 343 2555. E-mail: a.v.k.westwood@leeds.ac.uk (Aidan Westwood)
Present e-mail address for Li-Shang Lin: asimo945@gmail.com

use in photovoltaic devices and batteries as electrodes, next generation flexible electronics and even antibacterial coatings [1]–[3]. Of interest are the unique flexibility and tuneability of the properties of graphene- based materials [3], [4]. However, the term 'graphene' is often misused and difficulties in the large-scale production of true two-dimensional graphene have limited its applications [5], [6]. In the past decade, both bottom-up (i.e. chemical vapour deposition, synthesis via SiC) and top-down methods (i.e. solution-processed exfoliation, chemical oxidation, electrochemical exfoliation) have been developed to overcome this obstacle. However bottom-up methods are limited by their expense and the potential of top-down synthesis methods is restricted by quality control issues.

Liquid-phase graphite exfoliation (LPE) is considered a potential method for realising industrial-scale graphene production. This method generally refers to synthesis processes that involve separating graphite powder into graphene flakes by applying mechanical forces in a liquid, and the resultant graphene suspension can then be directly deposited onto a substrate to form a transparent conductive film [7]–[9]. Unfortunately, the LPE method cannot yet produce homogeneous fully delaminated two-dimensional graphene. Kauling's et al. systematic examination of graphene from 60 producers revealed that less than 10% of the material in most of the products tested consisted of graphene, with none of the products containing more than 50% [10]. Even then, such graphene is usually highly defective and contaminated, most likely as a result of the LPE methods [10], [11]. In other words, the majority of graphene products consist mainly of graphite powder rather than graphene flakes and it appears many graphene producers and/or researchers may be either unaware or perhaps insufficiently concerned about this. Therefore, unless a standardised characterisation protocol can be developed and practically implemented, research on graphene applications may never progress if such early development is based on the use of 'fake graphene'[10], [11].

A three-dimensional graphite needs to be delaminated completely in order to exhibit the full potential of two-dimensional graphene. Only single-layer graphene (SLG) and bilayer graphene (BLG) have the unique zero-bandgap electronic configuration, whilst in few-layer graphene (FLG), consisting of 3 to <10 layers, the conduction and valence bands begin to overlap. Thicker graphene structures should therefore be considered as thin film graphite instead of graphene [12]–[15].

Hence, rapid differentiation of "true graphene" is a critical task Although many analytical techniques have been continuously improved, methods to quantify rapidly the nano-structural features of graphene are still limited. This is due to the difficulties of visualising ultra-thin nano-flakes and the fact that many of the graphene properties which could be used to identify the material are still unknown [16]–[18]. Currently detailed graphene characterisation relies on direct examination using modern high-resolution transmission electron microscopy (HR-TEM), however this technique is limited in terms of its throughput, making large-scale, quantitative and statistically reliable data interpretation challenging. Atomic force microscopy (AFM) is an alternative technique which can be used to obtain various nanostructural features in a relatively faster manner, but thickness determination can be ambiguous due to the possiblity of hydrocarbon contamination and the existence of a buffered layer between the sample and substrate [19], [20]. Although photon-probe based spectroscopic techniques (such as Raman spectroscopy [21], reflection spectroscopy [22] or light scattering techniques [23]) do not directly image nanostructural features of graphene flakes, they can relatively rapidly differentiate graphene from graphite, based on graphene's unique optical and electronic properties [22], [24]. Howeveras many of the properties of graphene are still unclear, e.g. differing reported refractive index values unclear[17], [22], [25], such approaches often rely on the semi-empirical measurement of a series of well characterised graphene/graphite samples, making their precision and accuracy uncertain [26], [27]. Such studies have often been

calibrated using measurements on a few selected homogenous graphene flakes synthesised at the laboratory scale by either Chemical Vapour Deposition (CVD) or mechanical exfoliation. This may not be applicable to the LPE-synthesised graphene due to its inherently high inhomogeniety (i.e. variations in thickness, shape, defect concentration and lateral dimension), making characterisation of a few selected graphene flakes inappropriate [5], [23], [28].

This work elaborates upon the more limited techniques that were reported in reference [28] and has significantly extended the data analysis and cross-correlation of techniques. In this way, the present work presents a much more comprehensive methodology for characterisation of liquid phase synthesised heterogeneous graphene that now also includes assessment of defect density.

To characterise highly inhomogeneous LPE-synthesised graphene, Eigler et al. [29] introduced statistical techniques to study inhomogeneous graphene oxide (GO). Samples were firstly characterised by scanning Raman spectroscopy (SRS) and the results were then correlated to benchmark measurements determined by direct-imaging using AFM. With the determination of defect density distributions, a quantitative assessment and a more complete picture of the flake quality could be obtained [29]. However, the acquisition and processing of such a large amount of data is difficult and time consuming, making such a method inaccessible for rapid characterisation. Related studies have focused on the quantitative evaluation of flake lateral dimensions based on light scattering techniques. Lotya et al. [30] developed a method for the in-situ characterization of the lateral dimensions from dynamic light scattering (DLS), but the shape dependent fractional coefficient and the full lateral size distribution remained inaccessible. Walter et al. [23] obtained the lateral dimension distribution of graphene oxide (GO) by analytical ultracentrifugation (AUC), showing a very high correlation with the distribution obtained from atomic force microscopy (AFM). However, this was reliant on constant flake thicknesses (e.g., a fully delaminated graphene oxide sample was used) and the

suitability of applying such a method to determine the lateral size distribution of an unknown, mixed graphene/graphite suspension is open to question.

An ideal characterisation method should be able to differentiate thin graphene flakes from thicker graphite plates and provide quantitative information about the degree and quality of exfoliation, i.e. the flake thickness, the lateral dimension of the flake and the crystal imperfections. As shown schematically in figure 1, based on this quantitative information, a particular graphene synthesis process could be compared with other methods and also optimised. In addition this approach can also be used as a tool to understand the mechanisms of graphite exfoliation. As a result, the National Physical Laboratory (NPL) have published a Practical Guide for graphene characterisation [31], however a method that can be used to evaluate quantitatively the quality of graphene from a large-scale production process remains lacking.

There are differing relative merits for the various characterisation methods. The strength of electron probe-based techniques is that they allow characterisation of graphene in detail, but they are limited in terms of output, meaning it is diffcult to obtain statistically relevant data over large length scales. Photon probe-based techniques are relatively efficient for large length scale examination, but the acquired information is less direct due to the nanostructural features

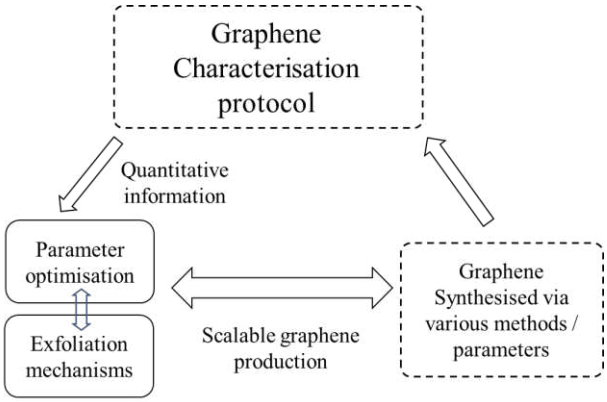

Figure 1: The need for a graphene characterisation protocol to assess scalable graphene production.

often being smaller than the wavelength of the incident radiation and the scattering events are therefore less localised as compared to electron probe-based techniques. As a result any experimental studies based on the photon probe techniques must rely on empirically measuring a series of samples [26]. Therefore the evaluation and accurate assessment of photon-probe techniques is the key step for their general application in the determination of graphene properties.

In this paper, using a commercial LPE graphene dispersion, initially we critically assess each of the various methods for characterisation of graphene flake lateral dimension, thickness and defect density: TEM, white-light optical microscopy (OM), AFM and Raman micro-spectroscopy. We then cross-correlate techniques in order to develop a rapid and universally applicable graphene characterisation protocol. Generally initial characterisation employed a direct imaging technique such as TEM or AFM, and results were then correlated with other rapid, but less direct methods (photon probe-based techniques such as OM and Raman spectroscopy) in order to identify their limitations. Based on the integration of quantification methods and their statistical analysis, we demonstrate a practical approach for developing a graphene characterisation protocol that retains access to the precision and accuracy of the various graphene characterisation techniques. Such a characterisation protocol can usefully quantify and differentiate between inhomogeneous solution-processed graphene samples and thus can be used for optimising scalable graphene synthesis processes [5].

2. Experimental Methodology

Figure 2 schematically illustrates the overall methodology used for evaluating the various graphene characterisation techniques. TEM imaging techniques were first carried out to determine the lateral dimension, defect concentration and thickness of exfoliated graphene /

graphite flakes. The analysed distributions were used as benchmarks for the other characterisation techniques (Figure 2 (1)). Secondly, measurements based on photon-probe techniques were performed on the same graphene sample; the distributions of the same nanostructural features were obtained by Raman spectroscopy and reflective optical microscopy (Figure 2 (2)). The statistical results obtained from each method were compared to each other and the absolute and relative deviations were calculated and are discussed in light of the techniques.

The same commercial 2Dtech^{TM} (aquagraph series[1]) graphene sample was used throughout this study. The 2Dtech^{TM} (aquagraph series) graphene sample was synthesised via exfoliation through milling in an ionic liquid. This wet ball-milling exfoliation is based on generating shear forces on raw graphite, initiated by the relative rotation between the milling balls, and breaking

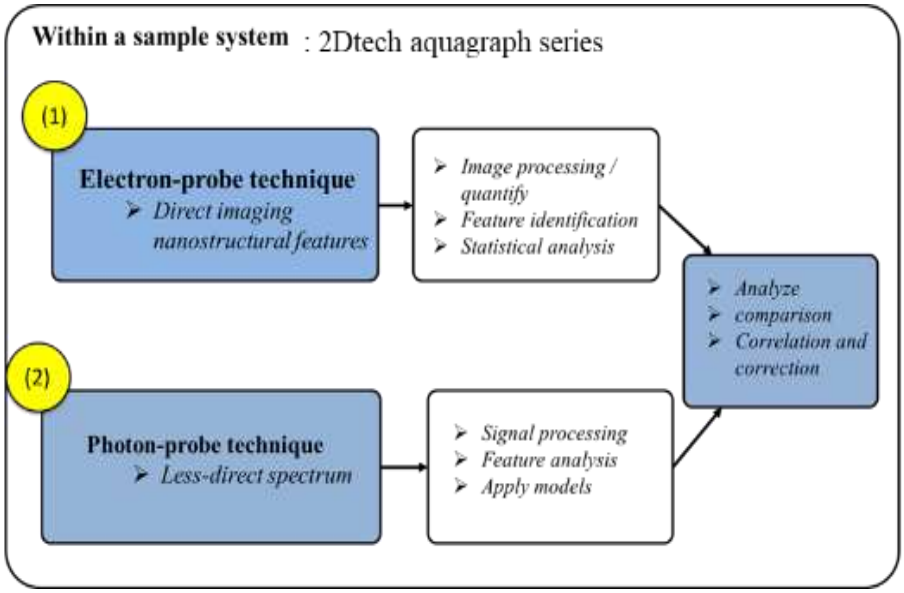

Figure 2: the general procedure to determine the distribution of nano-structural features in graphene dispersions.

[1] "2-DTech Graphene | Products." [Online]. Available: https://www.2-dtech.com/products/. [Accessed: 04-Oct-2019].

the weak van-der-Waals bonds between the graphite layers. The commercialised graphene sample was provided by 2Dtech^{TM} and was re-dispersed in isopropyl alcohol (IPA) before characterisation. A 300-second sonication (40 kHz, 80W) process was applied prior to each experiment to overcome any serious agglomeration. The resulting suspension was drop-cast onto holey carbon-coated TEM grids and SiO_2/Si substrates for TEM and optical microscopy, respectively. A monolayer CVD graphene[1] was used as a reference for Raman measurements, the sample was transferred onto a SiO_2/Si wafer substrate to visualise and locate the bulk and edge regions.

2.1 TEM characterisation

TEM measurements were conducted using a (monochromated) FEI Titan3 Themis 300 S/TEM operated at 80 kV which, for graphitic carbon, is below the threshold for knock-on damage [32]. Bright- field (BF) images were acquired using an objective aperture of 17.9 mrad and with the sample close to or along the <001> zone-axis (ZA). The transmitted electron intensity was measured using a Gatan Oneview Charged-Coupled Device (CCD) CMOS camera attached to the TEM. Electron energy loss spectroscopy (EELS) was undertaken with a Gatan Quantum 965 ER imaging filter, with the microscope in diffraction mode and a selected area aperture inserted. The convergence angle was 1.0 mrad and the collection angle was 5.4 mrad, this is close to the magic angle [33] in order to remove sample orientation effects. EEL spectra were recorded with an energy resolution of 0.53 eV and an energy dispersion of 0.025 eV/channel.

2.2 Optical Microscopy

As simulation work suggested a ~285nm thick SiO_2 layer can generate maximum contrast between graphene and the substrate under green or white light illumination, a Fabry-Perot structure was formed by thermally growing a 284.1 ± 0.8(nm) thick oxide layer on a Si-wafer.

An Olympus BX51 series reflection light microscope fitted with a 100x objective lens (N.A. = 0.95) and a 163 ms exposure time was used to obtain the optical images; the white balance and RGB colour ratio were optimised by the pre-installed AxioVision software before image recording.

2.3 Raman Micro-Spectroscopy

A Renishaw InVia series Raman spectrometer was used; the excitation laser wavelength and energy were 514nm and 20mW, focused by a 50X (N.A = 0.75) objective lens. Raman peaks were fitted using Lorentzian functions. The intensity ratio of the D and G Raman peaks was used to estimate the topological defect concentration. A correlation between D peak intensity and the Full-Width-Half-Maximum (FWHM) of the G peak was used to determine the major contribution to the D peak enhancement. The number of graphene layers was determined via a 2D band asymmetry analysis, based on Ferrari's previous work [24], for which the data was recorded under the same experimental conditions (514 nm laser excitation laser). The variation of the 2D band shape and peak position was quantified in terms of the number of graphene layers; the detailed peak fitting process and regression are described in the supplementary information, section S1.

2.4 Atomic Force microscopy (AFM)

Atomic force microscopy (AFM) imaging was carried out using a JPK NanoWizard III (JPK Instruments AG) operated in tapping mode under dry conditions. The graphene samples were drop cast onto a 285nm thick SiO_2/Si wafer substrate, the same as for the optical measurement, with a thick glass slide bonded under the substrate to avoid unwanted vibration when interacting with the tip. The tip was manufactured from highly doped silicon (Nano-sensors, Switzerland), having a radius of curvature < 10nm. The spring constant of the cantilever was 42 N/m with a resonant frequency at 330 kHz. A standard dissipation procedure was performed prior to each

measurement to avoid unwanted static charge on the tip. The AFM was operated in phase contrast mode to rapidly locate the region/flake of interest prior to each high-resolution height contrast measurement. The graphene flake lateral dimension, thickness and defect distribution were determined via a combination of Image J and a self-developed Matlab code, where global and adoptive local pixel thresholding algorithms were used to differentiate the objects from the background.

3. Assessment of the Individual Charactersation Methods

3.1 TEM analysis

The morphology and shape of graphene flakes was determined by bright-field (BF) TEM

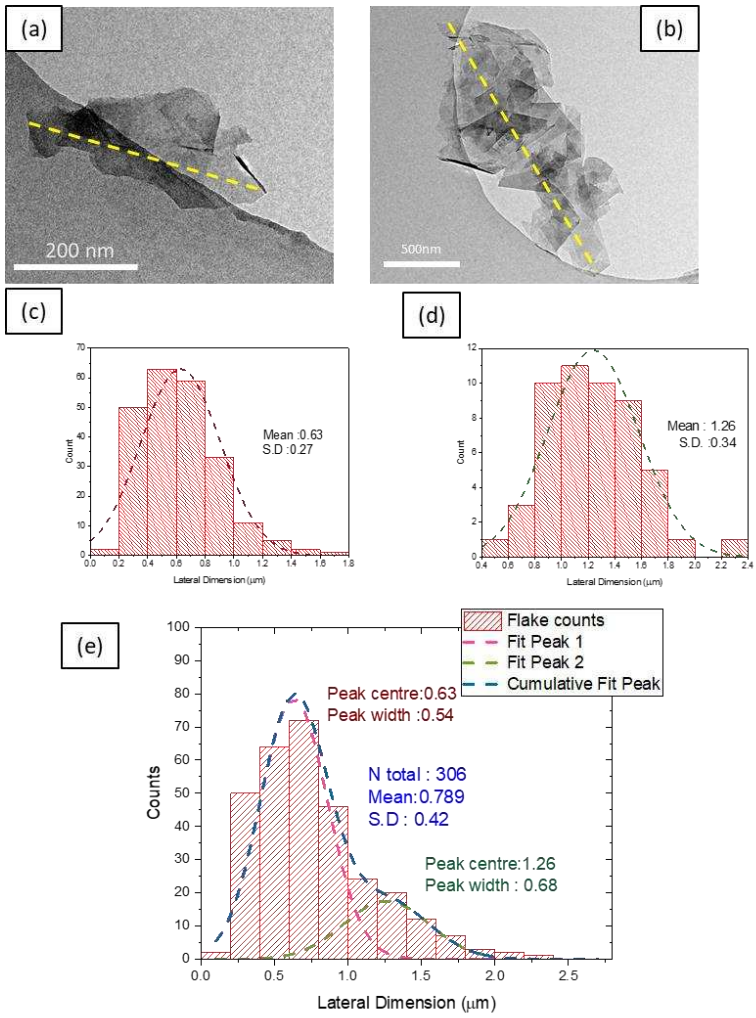

Figure 3: Bright field TEM images of (a) a primary graphene flake and (b) aggregated graphene flakes. The yellow lines in (a) and (b) illustrate the method used to determine the flake lateral dimension. The lateral dimension distributions of primary and aggregated flakes are shown in (c) and (d) respectively. (e) shows the histogram of the overall flake lateral dimension distribution. (2Dtech^{TM} graphene sample)

imaging. However, flakes were often aggregated or partially folded, complicating images and making them hard to quantify. Figure 3 (a) and (b) shows typical TEM images of primary and aggregated graphene flakes which were often suspended over a hole in the carbon support film. Selected graphene flakes were approximated as polygons and the Feret diameter was used for

lateral dimension measurement as illustrated by the yellow dashed-lines in figure 3 (a) and (b). Two types of flakes were evident: (a) primary and (b) aggregated, which resulted in a bimodal distribution curve as shown in figure 3 (e). The overall lateral dimension distribution was obtained from 306 flakes selected from several TEM images and gave a mean lateral flake size (for all selected flakes, consisting of both primary and aggregated flakes) of 0.78 ± 0.42 μm for sample population mean and standard deviation, where the best fit to the bimodal histogram was achieved using two Gaussian distributions, one peak centred at 0.63 μm with a peak width of 0.54 μm, and another Gaussian centred at 1.26 μm with a broader peak width of 0.68 μm. The result was confirmed by manually separating the primary and aggregated graphene flakes in the data analysis and measuring them independently. Primary flakes are fundamental flakes that cannot be separated into smaller flakes except by exfoliation, while aggregated flakes comprise two or more primary flakes attached together. Figure 3 (c) shows the lateral dimension distribution obtained from primary flakes, which ranged from c.a. 0.17 μm to 1.7 μm, with only two flake found to be smaller than 0.2μm. The mean lateral dimension of the primary flakes was 0.63 μm, the inhomogeneity of the flake lateral dimension exhibited a standard deviation of 0.27 μm, corresponding to the first Gaussian peak obtained in figure 3 (e) (red line). As shown in figure 3 (d), aggregated flakes exhibited a larger range in lateral dimension, from c.a. 0.4 μm to 2.4 μm, with > 98% bigger than 0.5 μm, a mean lateral size of 1.26 μm and a standard deviation of 0.34 μm, corresponding to the second Gaussian peak obtained in figure 3 (e) (green line).

Both BF TEM and dark field (DF) TEM imaging (the latter achieved by selecting solely diffracted beams with the objective aperture) can be used to identify crystalline regions with a specific crystal orientation, as well as structural imperfections such as in-plane defects and their spatial distribution [34]. This is used later in section 4.3.

The thickness of a graphene flake can be determined by one of three methods. Firstly, by counting the distinct (002) lattice fringes on the folded edge of the flake, where the graphene layers become parallel to the incident electron beam direction. This is often used as the main reference for other thickness estimation techniques due to its reliability [5]. A typical example of a folded graphene edge observed by HRTEM is shown in figure 4 (a). The fringes reflect the interlayer spacing of graphene, confirmed by the FFT diffractogram in figure 4(b) which revealed a periodicity of 0.34 nm (indicated by the red triangle). The FFT spot highlighted by

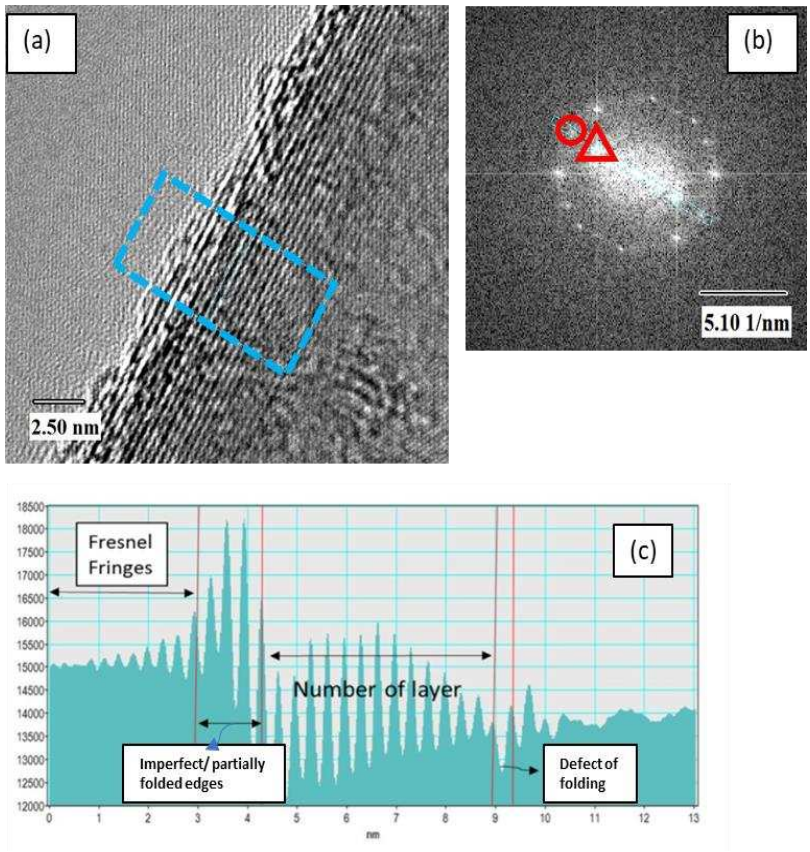

Figure 4: The use of folded graphene edges for the estimation of the number of graphene layers in a flake: (a) An example TEM image of a folded graphene edge; (b) FFT diffractogram showing the periodicity of 0.34 nm (red triangle), corresponding to the interlayer spacing of graphene; (c) Line profile corresponding to the blue rectangular in panel (a). The distance between peaks corresponds to the interlayer spacing and the number of peaks represents number of layers (14 in this case)

the red circle in figure 4 (b) corresponds to the {110} plane of the hexagonal sp^2 carbon lattice. The periodic interlayer spacing is also evident in the intensity profile across the HRTEM image

displayed in figure 4 (c) taken from the blue box in figure 4(a), from which an accurate number of graphene layers can be estimated by counting the number of fringes observed.

An alternative approach to thickness determination is via EELS measurements, where the thickness of specimen can be estimated from the EELS low loss spectrum and use of the conventional log-ratio method [33]. However, in practice, this method is of limited use for very thick specimens (thickness / inelastic mean free path ratios > 4) and also for very thin specimens. The latter arises due to the increasing dominance of surface plasmons in ultrathin samples (typically t < 10 nm) [35], [36] such as few layer graphene, which leads to an over-estimate of thickness. Further details of surface plasmons and how their influence on low loss spectra (particularly the position of the plasmon peaks) can be used to identify the thickness of few layer graphene samples is discussed in the Supporting Information (SI), section S3 However, in general EELS cannot be easily used as rapid means of measuring flake thickness over a range of flake thicknesses.

Scattering of the incident electron beam by the specimen produces mass-thickness contrast in the image and reduces the transmitted electron beam intensity. This can provide a rapid means of thickness determination using BF TEM images of graphene flakes. The transmitted beam intensity decreases as specimen thickness increases and is described by the dynamical theory [37], [38]. In the two beam, thin-film approximation, the normalised transmitted beam intensity $T(t)$ can be expressed as [37]:

$$T(t) = \frac{I_t}{I_0} = \left[1 - \frac{t}{\delta}\right] \dots (Equation.\,1)$$

where t is the specimen thickness in nm and the transmitted electron intensities I_t and I_0 correspond to the pixel intensity of a bright-Field (BF) image in a region of interest (ROI) on the sample and in the vacuum (i.e. over holes in the carbon support film), respectively. The parameter $\delta = \frac{\xi_0'}{2\pi}$ is the absorption constant for the material, where ξ_0' is the mean absorption distance [37]. A BFTEM image obtained in a near <001> zone-axis (ZA) orientation is shown in figure 5(a), and the transmitted BF intensity is measured using an objective aperture shown

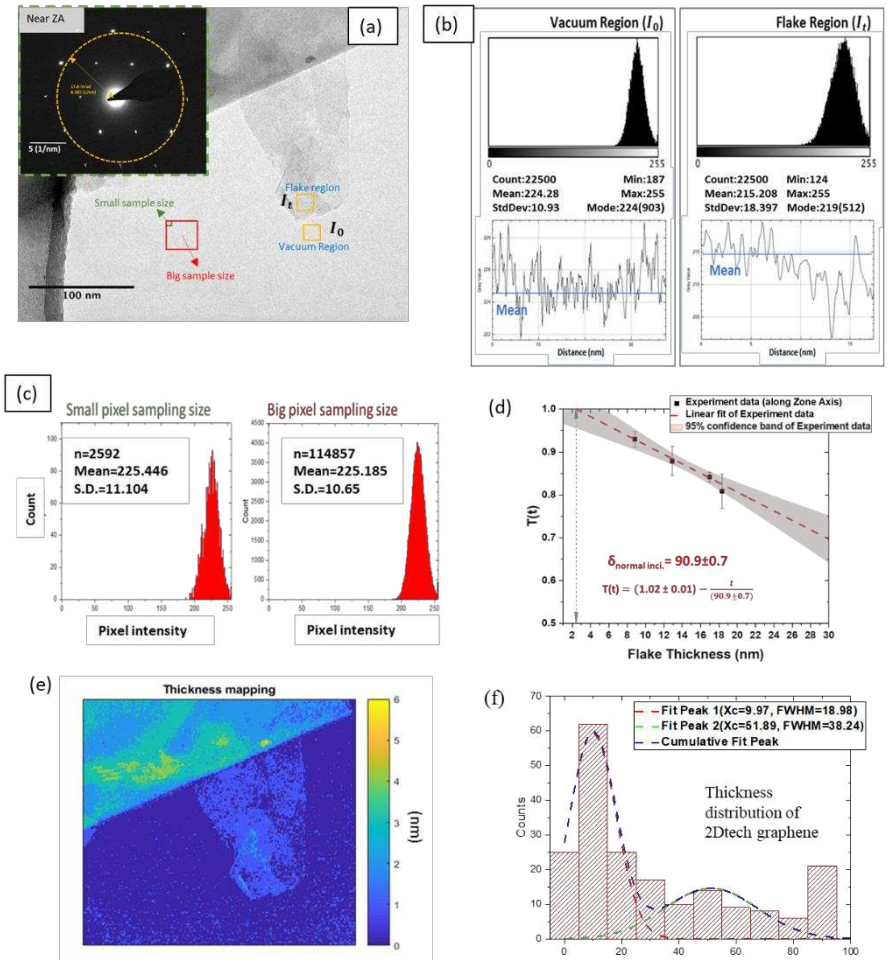

Figure 5: Extraction of information from BFTEM image contrast values. (a) and (b) show the difference in mean intensity value in vacuum and flake regions. The flake inhomogeneity is a problematic issue for such image sampling; (c) shows histograms of pixel intensity obtained from a vacuum region; the fluctuation can be significant when sampling size is too small as seen in the difference in standard deviation. The mean value will remain similar due to Centre Limit Theorem (CLT); (d) Plot of normalised transmitted intensity measured on <001> Zone axis (ZA) versus flake thickness obtained through direct imaging of the folded flake edge by HRTEM. The linear relationship exhibits a resolution limit of ~3 nm thickness (see dotted line); (e) Thickness map of the flake in (a) obtained via the application of equation 2; (f) Thickness distribution of the 2Dtech graphene sample obtained by the normalised BFTEM transmitted intensity method.

as dashed orange circle in the inset diffraction pattern. The flake regions are darker than the vacuum regions, indicating a lower electron transmission intensity, as quantitatively shown by the pixel intensity histograms in figure 5(b). Significant noise is evident in the pixel intensity profile in both vacuum and flake regions due to the contribution of random shot noise and flake inhomogeneity. Inhomogeneous regions on flakes arising from surface contamination or incomplete delamination have been widely observed in LPE graphene [20], [39]. The effect of shot noise can be minimised by averaging the pixel intensity over a larger ROI which samples more pixels in the image. Figure 5(c) shows histograms of the average pixel intensity obtained from a vacuum region. The distribution can be approximated by a Gaussian and the standard deviation represents the degree of signal fluctuation which, in this case, is dominated by the shot noise. A bigger ROI in the vacuum region results in a better defined standard deviation, but the mean pixel intensity value remains similar.

Figure 5 (d) shows the relationship between normalised transmitted intensity $T(t)$ and flake thickness. The normalised transmitted intensity $T(t)$ was obtained from an ROI of 150 ×150 pixels, as highlighted in figure 5(a), where the mean pixel intensity was measured both on and off a flake. A total of four flakes were selected, all of which exhibited folded edges. The values of $T(t)$ were plotted against the thickness determined by lattice imaging of the folded edge, and a linear relationship was obtained as:

$$T(t) = (1.02 \pm 0.01) - (0.011 \pm 0.001)t \ldots (equation. 2)$$

Despite the fact that our measurements were conducted near (rather than off) a ZA orientation, where the two beam approximation is not valid, equation 2 appears to confirm the linear relationship as described in equation 1 between the transmitted BF intensity and thickness, at least for thin flakes. Values of 1.02±0.01 and 0.011 ± 0.001 were obtained for the y-intercept and slope respectively. The former is slightly bigger than 1, indicating that this thickness

estimation method is inaccurate when the thickness of is < 3 nm. The slope of the plot can be used to extract the material-dependent absorption constant (δ) , where $\delta = 1/slope$ (comparing equations 1 and 2). The absorption constant in normal electron incidence was derived as $\delta_{normal.inci.}$= 90.91±0.67nm, which is lower than the absorption constant (δ_{exp} = 225 nm) derived by Rubino et al. [36] due to the presence of additional diffraction losses when the crystal is on or near a zone-axis (i.e. not a two beam case) [9], [37]. Using the derived values of $\delta_{normal.inci.}$ and the y-intercept, a thickness map of graphene can be obtained from an arbitrary BF-TEM image. Figure 5(e) shows an example of thickness mapping obtained via the application of equation 2. Figure 5(f)) shows the thickness distribution of 2Dtech graphene obtained via equation 2, using the selected flakes used for the lateral dimension measurements in figure 3. Overall this showed a mean normalised transmitted beam intensity of $T(t) = 0.8 \pm 0.36$, estimated to have a mean thickness t = 21 ± 33.1 nm using equation 2. However it displays a bimodal thickness distribution, in which the primary and aggregated graphene flakes, exhibited a sample population mean thicknesses of t= 10 ± 1.9 nm and t= 51 ± 10.7 nm, respectively. The aggregated graphene flakes were around five times the thickness of the primary flakes and resulted from the presence of folded flake edges and/or flakes stacking vertically on top of each other. However, the sensitivity of TEM diffraction contrast to bending and buckling of graphene flakes, the presence of uneven illumination, the interference from the holey carbon support film, as well as significant flake agglomeration, all mean that it is relatively difficult to apply this TEM image thickness mapping method for the general determination of flake thickness in dispersed graphene samples.

3.2 Quantitative optical imaging

Graphene characterisation via optical microscopy (OM) is a rapid and convenient method that can be adopted for large-scale graphene characterisation, refinement and optimisation. This technique relies on interference between light reflected from the material of interest and that reflected from an underlying substrate [40], [41]. Figure 6 (a) schematically shows the experimental set-up. A substrate with the Fabry–Perot structure is used - such a structure is formed from a set of parallel dielectric interfaces, in this case a known thickness of silica grown on a silicon substrate, whereby the frequency distribution of reflected light can be controlled by its path length. This structure, covered by dispersed graphene flakes of different lateral sizes and thicknesses, was illuminated by a white light-source with spectral intensity $I_{SR}(\lambda)$. The reflected light from the sample region can be categorized into that from the substrate

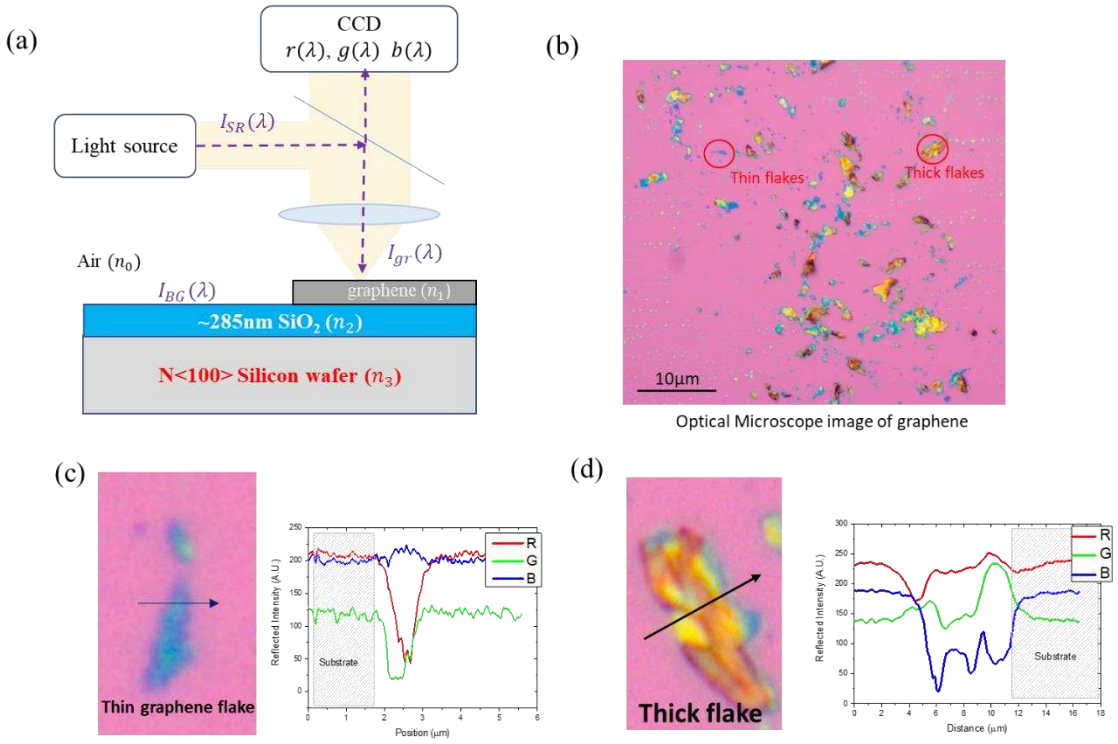

Figure 6: (a) Schematic diagram of the Fabry–Perot structure, comprising a silicon wafer with a silicon dioxide layer of a specific thickness (284.1 nm) optimised so as to enhance contrast between a graphene sample and the substrate; (b) reflected optical microscope image using 100X, NA=0.95 objective lens; (c) and (d) show the RGB channel split for thin and thick graphene flakes, respectively.

background $I_{BG}(\lambda)$ and that from the graphene flakes $I_{gr}(\lambda)$. The reflected light from the sample is collected and focused by lenses onto a detector, which converts the light into red, green and blue digital pixels. For a given light source, reflection spectrum and detector spectral sensitivity function, the absolute intensity of RGB pixels are given by integrating, over all wavelengths, the product of the spectral intensity of light reaching the detector (either from the substrate or the graphene film), the spectral intensity of the source and the respective (RGB) detector spectral sensitivity function [40].

The origin of the contrast between the background substrate and different flakes can be explained by Fresnel's equation, which considers the normal incident light from air ($n_0 = 1$) onto a graphene, SiO_2 and Si trilayer system [22], [41]. Then graphene flakes can be identified from their wavelength-dependent optical contrast as:

$$C(\lambda) = \left(\frac{I_{BG}(\lambda) - I_{gr}(\lambda)}{I_{BG}(\lambda)}\right) \dots (equation. 3)$$

Note, this equation is given in this particular form because thin (< ~10nm) graphene flakes reflect less green light than the background substrate (see figure 6(c)). The reflection spectra are functions of both thickness and refractive index of the material, with a detailed analysis including the variation of refractive index as a function of the number of graphene layers. Other potential factors such as the effect of lenses, the sensitivity of the CCD detector and other optical elements were constant in all experiments, similar to the thin-film calculations for normal incident light reported by Blake et al. and Ni et al [22], [41]. Thus for a given material and refractive index, along with illumination and camera characteristics, the expected pixel contrast between graphene and the substrate can be calculated [22], [41].

An OM image of graphene flakes is shown in figure 6 (b) and it is apparent that flakes exhibit

different colours. The lateral resolution of the OM setup was estimated to be 0.25±0.03 μm (see Supplementary information section S4), and the OM images were digitally split into red, green and blue (RGB) channels using a colour filter array based on the most commonly used Bayer pattern, implemented within a self-developed MATLAB code. The filters associated with the Bayer pattern have broad bandwidths nominally centred at 650nm, 550nm and 450 nm for the R, G and B channels respectively. The RGB intensity in the background region was relatively constant (Figure 6 (c)) while, for graphene flakes, each channel encountered notable changes (Figure 6 (d)). The proportion of reflected green light was considerably higher on thick flakes relative to thin flakes, resulting in a yellow- or brown-like colour, as opposed to the blue- or purple-like colour of thin flakes, in agreement with theoretical predictions [22], [41].

Figure 7(a) shows an AFM image of a graphene flake with a relatively large lateral dimension together with the corresponding OM image which is shown in figure 7(b). Figure 7(c) shows the RGB digital contrast in each channel as a function of flake thickness (as measured by AFM)**.** As discussed above, the green channel exhibited the most sensitivity to thickness, with contrast increasing as graphene thickness increased, making it ideal for thickness mapping. It should be noted that a negative value for the green channel contrast is due to the proportion of reflected green light being higher than the background (as is the case for thick flakes, see figure 6(d) and reference [22]). Thus thin (< ~10nm) graphene flakes can be selected by thresholding the green channel contrast > 0. Figure7(d) shows the green channel contrast map obtained from the image in figure 7(b), where the outline and shape of the graphene flake is evident. With 20×20 pixel sampling, the background substrate exhibited a mean reflection intensity of $I_{BG}(\lambda) = 82.71$, and the optical contrast from different parts of the graphene flakes can be calculated using equation 3. The measured thickness (by AFM) as a function of green channel contrast is shown in figure 7(e), and can be approximated by an exponential growth function:

$$t\,(C) = (-17.50 \pm 0.56) \times e^{\left(\frac{C(\lambda)}{-0.73 \pm 0.04}\right)} + (16.22 \pm 0.63) \ldots (equation.\,4)$$

where $t\,(C)$ is the flake thickness in nm, and $C(\lambda)$ the green channel contrast obtained from the OM image. Using equation 4, a thickness map of an arbitrary graphene flake can be obtained (Figure 7(f)). We note that a 1 nm thick region generates a contrast of only 0.1 in the green channel suggesting that thinner regions may be difficult to differentiate using this method.

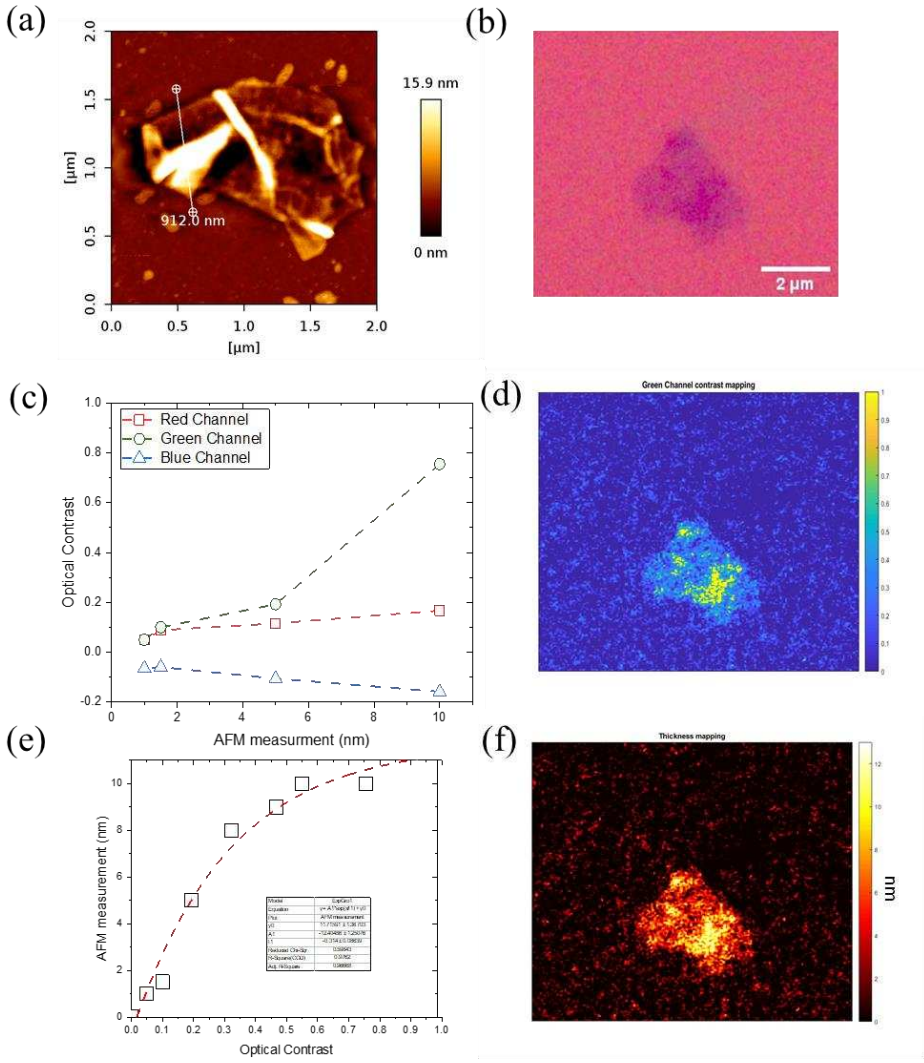

Figure 7: Comparison of flake thickness measurement by AFM and OM: (a) AFM image of a thin graphene flake; (b) OM image of the graphene flake; (c) Contrast of graphene as a function of thickness on 300 nm-thick SiO_2. The squares, dots and triangles are extracted from digital optical images with red, green and blue channels giving three separate values of contrast for each thickness measured by AFM; (d) shows the contrast map in the green channel obtained from (b); (e) Plot of the measured thickness as a function of green channel contrast; (f) the thickness map of the graphene flake obtained from the green channel contrast in (d).

Furthermore, owing to the presence of a buffer layer between the graphene flake and the substrate and/or the effect of distortion induced by the finite AFM tip radius, it has been reported that AFM will measure a limiting thickness of 1 nm, even for a single graphene monolayer [19], [20].

Despite this lack of precision in the AFM thickness measurement, the optical reflection spectrum method is able to resolve graphene regions as thin as ~ 1nm from the substrate. Even though precise thickness assessment remains slightly ambiguous, the ability to visualise thin samples is much higher than for other conventional optical techniques and the method can be used as a rapid screening tool to differentiate graphene flakes from thicker graphite flakes.

3.3 Raman micro-spectroscopy

Raman spectra were acquired from samples obtained by depositing graphene (both CVD and LPE graphene) onto the SiO_2/Si wafer substrate used for OM measurements. As shown in figure 8, the excitation energy (E_L)-independent G band is evident at ~1590 cm^{-1} and is related to first-order phonon scattering as expected in sp^2-bonded carbon materials, the relative intensity of this peak reflecting the degree of graphitisation [42]–[45]. The D band at ~1350 cm^{-1} is activated by the translational-symmetry breaking mode, which is related to the presence of defects, grain boundaries, functional groups or structural disorder [21], [46], [47]. Additional features such as the D' and D+D' peaks at ~1620 cm^{-1} and ~ 2940 cm^{-1}, respectively, are commonly observed in highly damaged graphene, arising from the presence of a high concentration of point defects or atom vacancies. The 2D band at around 2700 cm^{-1} originates from a second-order double resonance Raman process and exhibits a single Lorentzian peak with high intensity in pristine monolayer graphene regions, in contrast to the multimodal broad

peak observed in a 3-dimensional graphite (see figure 8 (a)). Therefore, the 2D band can be used, both as a signature for monolayer graphene and also to estimate the total number of layers in multilayer graphene, up to a total of 10 layers [18], [24]. A small peak at ~1450 cm^{-1} was also observed in the spectra shown in figure 8; this feature did not originate from the graphene sample, but from the third order Raman peak of the silicon substrate [47].

The intensity ratio between the D band and G band, (I(D)/I(G)), is often used to characterise the in-plane structural disorder of sp^2 carbon structures. Two well established models to correlate the I(D)/I(G) ratio to the quantity of disorder in the graphene basal planes are: (1) The Tuinstra–Koenig relationship [50], where the value of I(D)/I(G) is assumed to be due to grain boundaries between crystallites (or in this case graphene flake edges), and is inversely proportional to the basal-plane crystallite size (coherence length L_a) and; (2) The local activation model developed by Lucchese et al., where the zero-dimensional point defects in the bulk lattice are considered to be the major contribution to the D band and the concentration of point-defects within a graphene film (n_D) is dependent on the average distance between defects (L_D) with: $n_D \propto {}^{1}/_{L_D}$ [26], [51], and:

$$L_D{}^2(nm^2) = \frac{(4.3 \pm 1.3) \times 10^3}{E_L{}^4} \left(\frac{I_D}{I_G}\right)^{-1} \dots (equation\ 5)$$

As shown in figure 8 (a), a variation in the I(D)/I(G) ratio indicates differing concentrations of crystalline disorder between the various sp^2 carbon materials.

Since the shape and position of the Raman 2D peak changes as the number of graphene layers (N) increases, quantification of the 2D peak bandshape can be used to estimate the number of graphene layers constituting a flake [52]–[54]. However, the peak fitting process is complex and time consuming especially for the relatively weak 2D peak in damaged graphene [55], [56],

it being based on deconvolution of the 2D peak into four vibrational elements described in Supplementary Information S1. Thus, taking reference [55] as inspiration, an alternative simpler method based on analysing the 2D peak position was developed in order to simplify the characterization process.

In figure 8(b), the well-established spectral data of Ferrari [24] was taken for regression analysis, as it was recorded under the same experimental condition (514 nm excitation laser) [52]–[54]. As can be seen not only does the peak shape of the 2D band change with an increase in the number of graphene layers, but also the peak position shifts from ~2685 cm^{-1} in graphene to ~2725 cm^{-1} in graphite [52]–[54]. Information on the shifting of peak positions can be gathered by simple differentiation of the 2D peak, meaning that the requirement for a sharp 2D peak and a complex peak fitting process can be bypassed [5], [55], [56]. Figure 8 (c) plots both the 2D peak center and peak centroid as a function of number of graphene layers, using the data shown in figure 8 (b), in which the number of graphene layers were determined by TEM using the folded edge method [24]. For a monolayer and bilayer graphene flake, the 2D peak center and peak centroid are almost in the same position. This is due to the symmetrical peak shape of the 2D peak. The difference between the peak center and peak centroid position increases with the number of graphene layers, since the peak shape becomes asymmetric as in graphite. The relationship between peak centre and the number of graphene layers can be fitted with an exponential growth function, where the number of graphene layers can be estimated via an empirical equation:

$$N = (-1.94 \pm 0.23) \times ln\left(\frac{\left((2725.57 \pm 0.39) - X_c\right)}{65.4 \pm 4.96}\right) \ldots (equation\ 6)$$

where X_c is the position of peak centre and N is the number of graphene layers in the flake of interest.

Figure 8 (d)-(g) shows the results of Raman measurement of 20 randomly selected thin LPE graphene flakes from the 2Dtech sample. Overall these flakes exhibited a mean I(D)/I(G) ratio of 0.16 and a standard deviation of 0.053 (see histogram in figure 8 (d)). A linear regression was applied to correlate the FWHM (G peak) to the I(D)/I(G) ratio, where a Pearson's r value of 0.311 was obtained, indicating a weak correlation, as shown in the scatter plot in figure 8 (e)). The D band enhancement must therefore largely result from the presence of graphene flake edges rather than defects within the bulk [44], [51], [57], [58] . Figure 8(f) shows the histogram of the 2D peak position acquired from these selected graphene flakes. The center of 2D peak ranged from 2699 cm^{-1} to 2725 cm^{-1}, but no intense 2D peak centered at 2685 cm^{-1} was observed, indicating that clean monolayer graphene flakes were absent in the sample. Around half (47.6%) of these selected flakes exhibited a 2D band at a frequency > 2720 cm^{-1}, indicating many of these graphene flakes were incompletely delaminated and remained graphitic or possessed multilayer graphene properties. The thickness was estimated via equation 6 and the thickness distribution is shown in figure 8 (g) and exhibited a log-normal distribution. The

mean flake thickness was estimated to be between 5-6 layers, in which the population mean was estimated to be between 4-8 layers (detailed in supporting information S2). This mean flake thickness is smaller than that assessed by TEM analysis in Section 3.1 since the TEM analysis results in a measurement of physical thickness that, unlike the Raman analysis, includes regions of poor registry between layers as present in multilayer turbostratic graphene flakes. However, a significant proportion (23.8%) of these flakes were categorized as graphite as the estimated number of graphene layers were larger than 10 (N>10).

Overall, the analytical method based on deconvolution of the 2D peak is the most precise way to describe the variation in the Raman 2D band versus the number of graphene layers, because the method not only considers the shift in peak position, but also the 2D band broadening and differing relative contributions of separate peak intensities. However, the process is

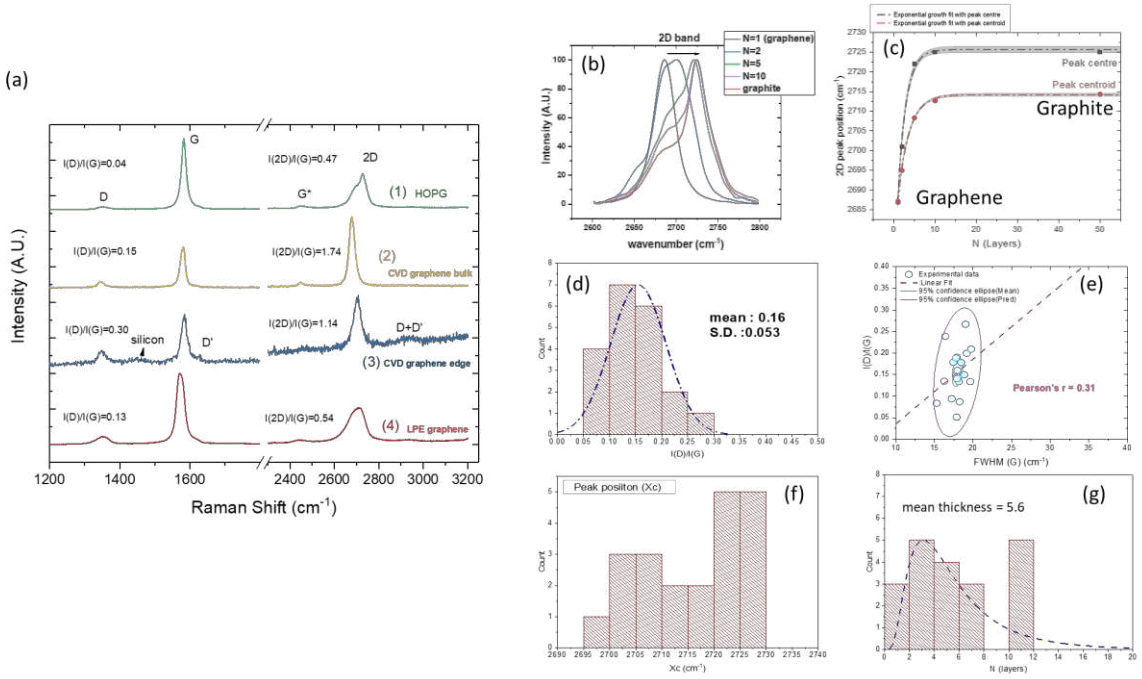

Figure 8: (a) Raman spectra measured from a CVD graphene bulk region and a region surrounded by graphene edges as compared with HOPG and LPE graphene; (b) Ferrari's data showing variation in the 2D band with number of graphene layers (c) Raman 2D peak position (both centre and centroid) as a function of number of graphene layers. The dashed lines show an exponential fit to the curves; (d) The distribution of I(D)/I(G) ratios from flakes in the 2Dtech graphene sample; (e) correlation between the I(D)/I(G) intensity ratio and the width of G band; (f) histogram of the 2D peak position acquired from the 2Dtech graphene flakes; (g) thickness distribution obtained using equation 9.

complicated and time consuming. Equation 6 provides a comparatively more simple method and, even though the method generally underestimates thickness, the difference is found to be small [5], [52]–[54].

4. Cross Correlation of Methods to Determine Graphene Sample Characteristics

4.1 Measurement of lateral flake dimension

To obtain reliable statistics for the overall lateral size distribution of thin graphene flakes from the 2Dtech sample, a number of optical microscope images were analysed. The green channel contrast was used to filter the thin flakes from both the background and the thick (> ~10nm) flakes. Graphene flakes that had green channel contrast values of between 0.020 and 1 were chosen, and a total of 6572 thin flakes with a lateral size > 0.2 μm were selected for statistical analysis. Section S5 in the Supporting Information discusses the precision of lateral size measurement using this method. A representative optical image is shown in figure 9 (a). The analysed image gave a population mean lateral size of $< L > = 0.8 \pm 0.4$μm, as shown in figure 9(b), where the raw histogram of the size distribution and cumulative flake size percentage are plotted. The distribution histogram can be fitted by two Gaussian distributions, which are plotted and analysed in figure 9(c). One Gaussian peak is located at 0.62 μm, with a peak width of 0.37 μm (indicated by the red line). The second Gaussian peak is located at 1.24 μm and exhibits a broader peak width of 0.49 μm (indicated by the green line). The broadening and asymmetric lateral size distribution can be explained by the presence of both primary graphene flakes and aggregated flakes lying on the substrate [59]. The unintentional selection of both primary flakes and aggregated flakes is because of the lack of resolution of the technique. Figure 9(d) shows a plot of the histogram fitted with a log-normal function. This log-normal

histogram shows a more symmetric distribution, especially for flake sizes < 1.1µm. This suggests that aggregation is a result of coalescence, presumably with the graphene flakes having a tendency to stack vertically rather than horizontally.

Figure 9 (e) shows a comparison of the lateral size distributions obtained by both optical microscopy and TEM (the latter taken from figure 3(e)), where the flake counts have been normalised and expressed as a number percentage. From OM analysis, the primary Gaussian

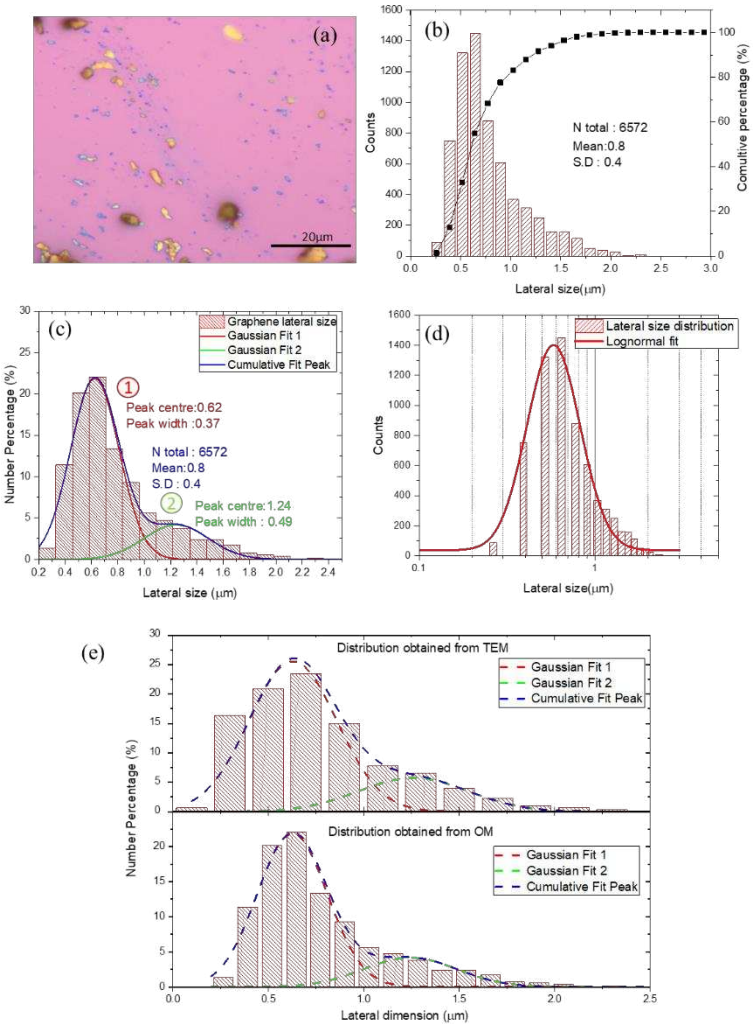

Figure 9: (a) shows an OM image of thin and thick graphene flakes deposited onto an SiO_2/Si wafer substrate via drop casting; (b) Cumulative percentage and histogram of lateral dimension distribution for 6572 selected flakes; (c) The data was fitted with multi-Gaussian function with two individual Gaussians. Peak 1 represents the lateral dimension distribution of primary flakes and peak 2 represents aggregated flakes; (d) When the distribution was fitted with a lognormal distribution a single symmetric distribution is obtained; (e) Comparison of the lateral dimension distributions obtained by TEM and OM.

peak is centred at 0.62μm which corresponds to the primary peak at 0.63μm obtained from TEM, indicating a difference of only 1.6 %. The secondary peak from OM analysis is a Gaussian peak centred at 1.26 μm, a difference of 0.8 % compared to the TEM observations. The median value for lateral flake size from TEM is 0.708 μm, 0.041 μm larger than the value obtained from OM. This highlights the difference in flake identification efficiency between the OM and the TEM methods. In TEM, more flakes were categorised as aggregates and this number of aggregates was taken into account by the statistics, resulting in a larger median number. Nevertheless, the comparison suggests that the distribution in the lateral size of graphene flakes can be readily extracted from the quantitative optical image analysis technique which can provide sufficient and reliable statistics for a sample. Only a small difference with the TEM observation is found, which implies that the lateral size distribution of sub-micrometre graphene flakes can be effectively obtained via this method. Observation of a bimodal flake size distribution indicates that both primary flakes and aggregated flakes were included even when thicker flakes were deliberately excluded during the OM flake selection process, meaning that the current selection technique does not have the capacity to differentiate primary flakes from the aggregated flakes with a high degree of detail.

4.2 Thickness mapping

AFM measurements of the 2Dtech LPE graphene sample are shown in figure 10 (a). The results were obtained on a 285nm thick SiO_2/Si wafer substrate, and very thick islands were avoided using the optical microscope, so that the AFM cantilever could be operated over a small height range; thus, measurement was biased toward thinner flakes. Figure 10(b) plots the height profiles of some example flakes. Height fluctuations were evident possibly due to the presence of contamination (i.e. possible hydrocarbon contaminants on the graphene surface [20], [60], [61]) or surface roughness. However, the fluctuations always occurred on a plateau region with

a discrete step height (e.g. 1, 2, 3 nm… etc), which can be explained by the existence of a buffer layer between the graphene and the substrate. The buffer layer is due to capillary flow on the Si/SiO_2 substrate which is formed as a result of an increase in flake concentration during solvent evaporation and cannot be avoided during the drop-casting step. However, such capillary solvent may not have been expelled even when the flakes reaggregate, leading to a non-linear progression for the height measurements from monolayer to multilayer graphene, where stronger interlayer forces in incompletely delaminated multilayer graphene result in a smaller step change in height as compared to that in re-aggregated graphene [23]. Virtually no literature has reported a 0.34 nm step height representing the interlayer spacing in LPE graphene samples [19], whereas, in contrast, a 0.34 nm interlayer spacing has been observed in an incompletely delaminated flakes synthesised by mechanical exfoliation [19]. Figure 10(c) shows the thickness distribution obtained from AFM images of a total of 48 flakes which showed a population mean thickness value of 3.11±0.02 nm (i.e. the confidence interval of the population mean is $2.8 < \mu_{thickness} < 3.4$) . Assuming the buffer layer to be present only between the substrate and the graphene flakes, and that this layer is 1 nm thick, these graphene flakes could therefore be approximately 6-8 layers thick.

Figure 10 (d) shows thickness distribution of 2Dtech graphene flakes obtained by quantitative optical mapping of over 6000 flakes using equation 3. Thick flakes outside the contrast range of $0.020 < C(\lambda) < 1$ were excluded. These were the same selected flakes that were used for lateral dimension statistics in figure 9. The results revealed that the sample population mean thickness was 3±1nm, with the histogram showing a bimodal distribution with peaks centred at 2.3 nm and 6.7 nm. The bimodal thickness distribution is due to the presence of

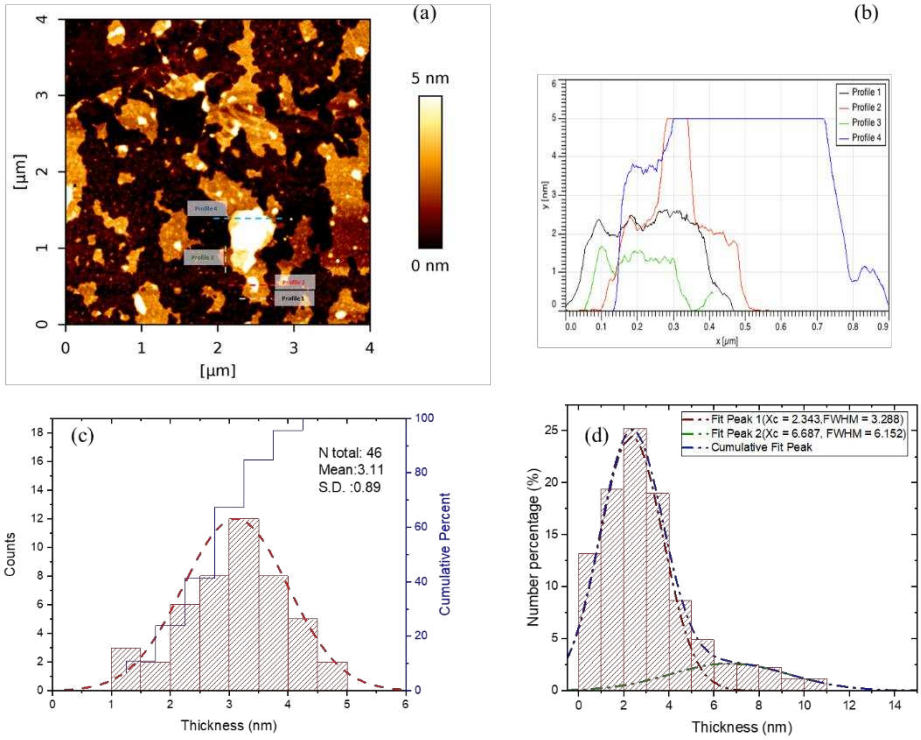

Figure 10: Compares the thickness distribution measurement obtained by AFM and quantitative optical mapping: (a) an AFM image of the 2Dtech graphene sample; (b) the height profiles of example graphene flakes; (c) shows the thickness distribution obtained from the AFM images; (d) the thickness distribution obtained by quantitative optical mapping.

agglomeration. The results obtained by quantitative optical mapping agreed well with the AFM results (where 48 flakes were measured), but demonstrated a significant discrepancy when compared to the TEM normalised transmission intensity method (see section 3.1, where 306 flakes were measured). This is probably due to the factors mentioned previously in section 3.1, as well as the folding or curling of flake edges (see figures 3(a) and 3(b)), which make it difficult to apply the TEM image thickness mapping method for large-scale thickness

determination. Furthermore, there was no real well-defined selection procedure in terms of exactly which flakes were analysed for thickness by TEM.

As mentioned earlier when discussing figure 8 (g), a mean 5.6 graphene layers with a standard deviation of 3.4 layers gives the population mean in the interval of 4-8 layers (i.e. 1.2 - 2.4 nm thick) was the thickness estimated for the 2Dtech aquagraph sample using Raman spectroscopy. This is similar to the observations using OM and AFM on the same sample (i.e. mean values of 3.11 nm and 3±1 nm for AFM and OM, respectively). It should be noted that Raman spectroscopy cannot differentiate flakes with thicknesses >> 10 layers, resulting in statistics that are therefore biased in favour of thinner flakes. However thick flakes were avoided when performing the OM and AFM measurements, resulting in differences between the number of graphene layers estimated via OM, AFM and Raman being small.

Overall a precise thickness characterisation method is difficult to achieve for large-scale measurement. Nevertheless, despite it being difficult to ascertain the precise number of graphene layers over a range of flake thicknesses, identifying the approximate thickness distribution and the degree of graphitic character is probably a more practical and important aspect in terms of improving a particular graphene synthesis process. Therefore, analysis of the position of the Raman 2D band is probably the most practical technique that can be used to determine the degree of graphitic character, and the number of coupled layers.

4.3 Measuring Defect Concentrations in Graphene Flakes

To assess the reliability of using the Raman I(D)/I(G) peak ratio to assess the degree of crystal imperfection in graphene flakes, the average distance between defects (L_D) was calculated via

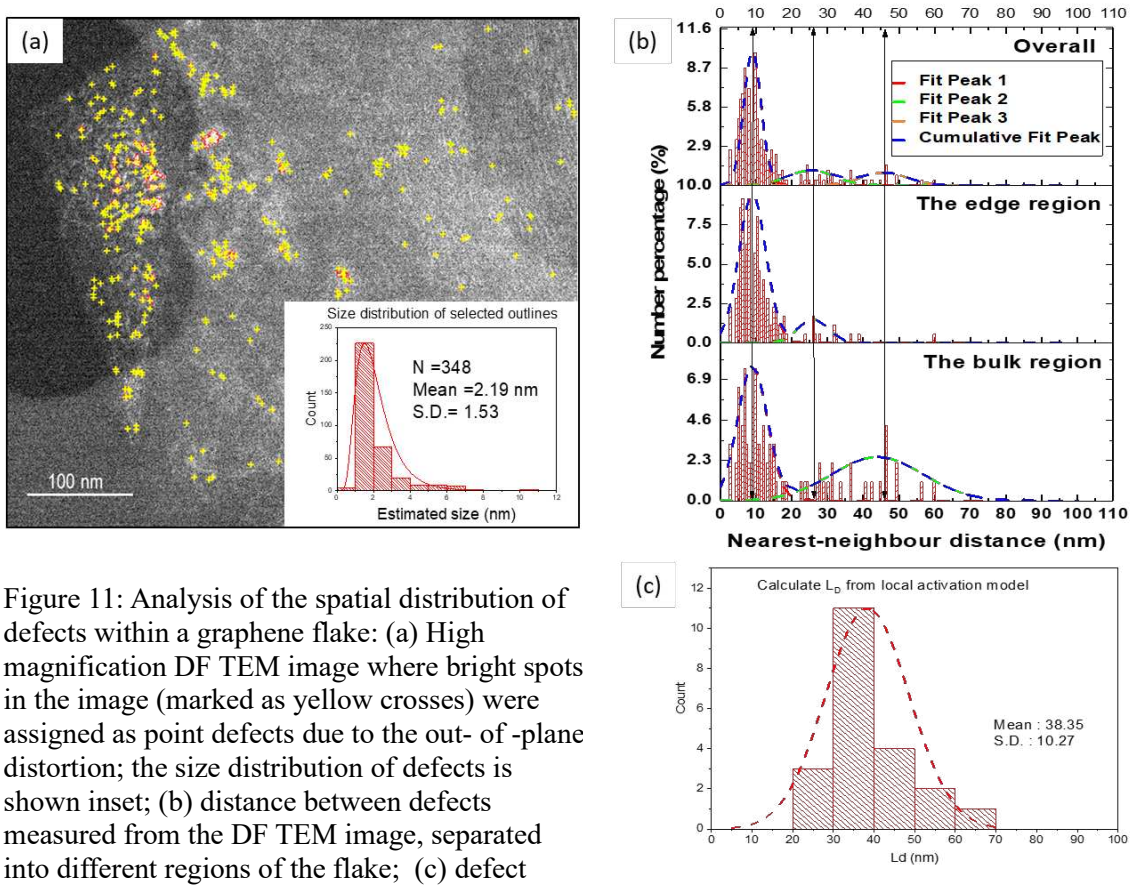

Figure 11: Analysis of the spatial distribution of defects within a graphene flake: (a) High magnification DF TEM image where bright spots in the image (marked as yellow crosses) were assigned as point defects due to the out- of -plane distortion; the size distribution of defects is shown inset; (b) distance between defects measured from the DF TEM image, separated into different regions of the flake; (c) defect distribution from Raman spectroscopy obtained by estimating L_D using the local activation model and equation (5).

the local activation model and equation (5) using measurements on 20 flakes in total. These results were then compared to the spatial distribution of defects obtained by DF TEM image analysis on 5 flakes. Note a TEM image is a two dimensional (2D) projection of a three dimensional (3D) structure, however for an ultrathin sample the distance between defects in a 2D projection should approximate to the real 3D distance. Results are shown in figure 11. The average L_D was estimated to be 38.35 nm using Raman spectroscopy and the local activation model (Figure 11(c)). However a multi-modal distribution was obtained from the nearest-neighbour distances between defects as determined using DF TEM image analysis (see figures 11 (a) and (b) which separates the defects into those near the edges of flakes and those within the bulk of the flakes). This multi-modal distribution consists of a large peak for short nearest-neighbour distances and a smaller peak for longer distances. The former represents clustered

defects that have an average separation of ~10 nm and may not be distinguishable by conventional Raman spectroscopy [26]. The defects separated by longer distances are distributed between ~20 to ~40 nm apart, a value similar in magnitude to the value of L_D estimated by the local activation model. This comparison also shows that an exact spatial distribution of defects cannot be obtained by Raman spectroscopy. The defect density estimation from the local activation model underestimated the defect concentration in the edge regions, but overestimated the defect concentration in the bulk regions.

5. Conclusions

In this paper, a characterisation protocol has been proposed to quantify the fundamental nano-structural features of graphene flakes, including: the lateral flake dimension, the flake thickness and degree of crystalline imperfection, all of which are important factors that determine the properties of a graphene sample, particularly those produced by liquid phase exfoliation. In all cases, these nano-structural features were initially characterised by the most precise technique based on direct imaging from TEM or AFM, the results then being used as benchmarks for faster, yet less direct methods based on photon-probe techniques. In order to integrate and assess the different characterisation techniques, all results have been quantified and statistically analysed.

It was found that the lateral dimension distribution of an LPE graphene sample could be rapidly obtained by quantitative analysis of optical micrographs, where a good correlation with TEM results was obtained with an error of 0.9% and 0.5% for the mean value of the primary flake and aggregated flake sizes, respectively. Also, by using the green channel contrast in the OM image, the distribution of flake thicknesses could be rapidly obtained. This showed a mean flake thickness which correlated well with AFM measurements. In addition, we have

characterized these graphene flakes using conventional Raman spectroscopy, from which both the number of graphene layers and distribution of crystalline imperfections within graphene flakes can be calculated. These results showed a good correlation with both AFM and DF TEM results respectively.

In summary, the proposed graphene characterisation protocol offers a practical method to integrate and evaluate the different characterisation techniques. This protocol has the ability to quantify and differentiate between inhomogeneous solution-processed graphene samples and can be used for optimising graphene synthesis processes. Furthermore, the protocol development method can be used as a reference point, which can be applied to other exfoliated materials for developing material-specific characterisation protocols that can rapidly assess the effectiveness of different parameters in the optimisation of processing routes.

Acknowledgements

The authors acknowledge the provision of facilities and technical support by the University of Leeds, particularly the Leeds Electron Microscope And Spectroscopy centre (LEMAS). Some of the experiments were perfomed in the Research Centre of Applied Science (RCAS) in Academia Sinica, Taiwan and the graphene sample was kindly provided by 2DTech™ .

References

[1] K. S. Novoselov *et al.*, "A roadmap for graphene," *Nature*, vol. 490, no. 7419, pp. 192–200, Oct. 2012.

[2] B. Pollard, "Growing Graphene via Chemical Vapor Deposition," *Ph. D. Thesis*, pp. 1–47, 2011.

[3] M. Hofmann, W.-Y. Y. Chiang, T. D Nguyn, Y.-P. P. Hsieh, T. D. Nguyễn, and Y.-P. P. Hsieh, "Controlling the properties of graphene produced by electrochemical exfoliation," *Nanotechnology*, vol. 26, no. 33, p. 335607, Aug. 2015.

[4] K. Parvez *et al.*, "Electrochemically exfoliated graphene as solution-processable, highly conductive electrodes for organic electronics," *ACS Nano*, vol. 7, no. 4, pp. 3598–606, Apr. 2013.

[5] L.-S. Lin, "Characterisation Protocol for Liquid- Phase-Synthesised Graphene," University of Leeds, 2018.

[6] J. H. Warner *et al.*, *Graphene : fundamentals and emergent applications*, 1st ed., vol. 17. Elsevier, 2013.

[7] E. B. Secor, P. L. Prabhumirashi, K. Puntambekar, M. L. Geier, and M. C. Hersam, "Inkjet printing of high conductivity, flexible graphene patterns," *J. Phys. Chem. Lett.*, vol. 4, no. 8, pp. 1347–1351, 2013.

[8] U. Khan, A. O'Neill, M. Lotya, S. De, and J. N. Coleman, "High-concentration solvent exfoliation of graphene," *Small*, vol. 6, no. 7, pp. 864–871, 2010.

[9] Y. Hernandez *et al.*, "High-yield production of graphene by liquid-phase exfoliation of graphite," *Nat. Nanotechnol.*, vol. 3, no. 9, pp. 563–568, Sep. 2008.

[10] A. P. Kauling *et al.*, "The Worldwide Graphene Flake Production," *Adv. Mater.*, vol. 30, no. 44, p. 1803784, Nov. 2018.

[11] P. Bøggild, "The war on fake graphene," *Nature*, vol. 562, no. 7728, pp. 502–503, Oct. 2018.

[12] K. S. Novoselov *et al.*, "Two-dimensional gas of massless Dirac fermions in graphene.," *Nature*, vol. 438, no. 7065, pp. 197–200, Nov. 2005.

[13] A. K. Geim and K. S. Novoselov, "The rise of graphene," Nature Publishing Group, 2007.

[14] S. V. Morozov, K. S. Novoselov, F. Schedin, D. Jiang, A. A. Firsov, and A. K. Geim, "Two-dimensional electron and hole gases at the surface of graphite," *Phys. Rev. B - Condens. Matter Mater. Phys.*, vol. 72, no. 20, p. 201401, Nov. 2005.

[15] B. Partoens and F. M. Peeters, "From graphene to graphite: Electronic structure around the K point," *Phys. Rev. B - Condens. Matter Mater. Phys.*, vol. 74, no. 7, p. 075404, Aug. 2006.

[16] H. Li *et al.*, "Rapid and reliable thickness identification of two-dimensional nanosheets using optical microscopy," *ACS Nano*, vol. 7, no. 11, pp. 10344–10353, 2013.

[17] M. Bruna and S. Borini, "Optical constants of graphene layers in the visible range," *Appl.*

Phys. Lett., vol. 94, no. 3, pp. 1–4, 2009.

[18] K. F. Mak, M. Y. Sfeir, J. A. Misewich, and T. F. Heinz, "The evolution of electronic structure in few-layer graphene revealed by optical spectroscopy.," *Proc. Natl. Acad. Sci. U. S. A.*, vol. 107, no. 34, pp. 14999–5004, Aug. 2010.

[19] J.-S. S. Kim *et al.*, "Between scylla and charybdis: Hydrophobic graphene-guided water diffusion on hydrophilic substrates," *Sci. Rep.*, vol. 3, no. 1, p. 2309, Dec. 2013.

[20] C. J. Shearer, A. D. Slattery, A. J. Stapleton, J. G. Shapter, and C. T. Gibson, "Accurate thickness measurement of graphene," *Nanotechnology*, vol. 27, no. 12, p. 125704, Mar. 2016.

[21] R. Beams *et al.*, "Raman characterization of defects and dopants in graphene," *J. Phys. Condens. Matter*, vol. 27, no. 8, pp. 83002–26, 2015.

[22] Z. H. Ni *et al.*, "Graphene thickness determination using reflection and contrast spectroscopy.," *Nano Lett.*, vol. 7, no. 9, pp. 2758–63, Sep. 2007.

[23] J. Walter, T. J. Nacken, C. Damm, T. Thajudeen, S. Eigler, and W. Peukert, "Determination of the lateral dimension of graphene oxide nanosheets using analytical ultracentrifugation," *Small*, vol. 11, no. 7, pp. 814–825, 2015.

[24] A. C. Ferrari *et al.*, "Raman Spectrum of Graphene and Graphene Layers," *Phys. Rev. Lett.*, vol. 97, no. 18, p. 187401, Oct. 2006.

[25] F. J. Nelson, V. K. Kamineni, T. Zhang, E. S. Comfort, J. U. Lee, and A. C. Diebold, "Optical properties of large-area polycrystalline chemical vapor deposited graphene by spectroscopic ellipsometry," *Appl. Phys. Lett.*, vol. 97, no. 25, p. 253110, Dec. 2010.

[26] L. G. Cançado *et al.*, "Quantifying defects in graphene via Raman spectroscopy at different excitation energies," *Nano Lett.*, vol. 11, no. 8, pp. 3190–3196, Aug. 2011.

[27] S. Reich and C. Thomsen, "Raman spectroscopy of graphite.," *Philos. Trans. A. Math. Phys. Eng. Sci.*, vol. 362, no. 1824, pp. 2271–88, Nov. 2004.

[28] L. S. Lin, W. Bin-Tay, Z. Aslam, A. V. K. Westwood, and R. Brydson, "Determination of the lateral size and thickness of solution-processed graphene flakes," *J. Phys. Conf. Ser.*, vol. 902, no. 1, 2017.

[29] S. Eigler, F. Hof, M. Enzelberger-Heim, S. Grimm, P. Muller, and A. Hirsch, "Statistical-Raman-Microscopy and Atomic-Force-Microscopy on Heterogeneous Graphene Obtained after Reduction of Graphene Oxide," *J. Phys. Chem. C*, 2014.

[30] M. Lotya, A. Rakovich, J. F. Donegan, and J. N. Coleman, "Measuring the lateral size of liquid-exfoliated nanosheets with dynamic light scattering.," *Nanotechnology*, vol. 24, no. 26, p. 265703, Jul. 2013.

[31] A. J. Pollard *et al.*, "Characterisation of the structure of graphene - Good pratictice guide N. 145," vol. 1, pp. 1–77, 2017.

[32] F. Banhart and F. Banhart, "Irradiation effects in carbon nanostructures," *Rep. Prog. Phys.*, vol. 62, no. 8, p. 1181, Aug. 1999.

[33] R. Egerton, *Electron Energy-loss Spectroscopy in the Electron Microscope*. Springer, 2014.

[34] M. Y. Na, S. Lee, D. H. Kim, and H. J. Chang, "Dark-field Transmission Electron Microscopy Imaging Technique to Visualize the Local Structure of Two-dimensional

Material ; Graphene," vol. 45, no. 1, pp. 23–31, 2015.

[35] C. B. Williams, David B., Carter, *Transmission Electron Microscopy - A Textbook for Materials Science | Springer*. Springer; 2nd ed. 2009 edition (27 Aug. 2009).

[36] R. F. Egerton, "TEM Applications of EELS," in *Electron Energy-Loss Spectroscopy in the Electron Microscope*, Boston, MA: Springer US, 2011, pp. 293–397.

[37] S. Rubino, S. Akhtar, and K. Leifer, "A Simple Transmission Electron Microscopy Method for Fast Thickness Characterization of Suspended Graphene and Graphite Flakes," *Microsc. Microanal.*, vol. 22, no. 01, pp. 250–256, Oct. 2016.

[38] L. Reimer H. Kohl, L. Reimer, and H. Kohl, *Transmission Electron Microscopy :Physics of Image Formation*. Springer Verlag, 2008.

[39] X. Liu, I. Balla, H. Bergeron, and M. C. Hersam, "Point Defects and Grain Boundaries in Rotationally Commensurate MoS 2 on Epitaxial Graphene," *J. Phys. Chem. C*, vol. 120, no. 37, pp. 20798–20805, Apr. 2016.

[40] B. S. Jessen *et al.*, "Quantitative optical mapping of two-dimensional materials," *Sci. Rep.*, vol. 8, no. 1, pp. 2–9, 2018.

[41] P. Blake *et al.*, "Making graphene visible," *Appl. Phys. Lett.*, vol. 91, no. 6, p. 063124, May 2007.

[42] A. Jorio, M. S. Dresselhaus, R. Saito, and G. Dresselhaus, *Raman Spectroscopy in Graphene Related Systems*. Wiley, 2011.

[43] M. Huang, H. Yan, C. Chen, D. Song, T. F. Heinz, and J. Hone, "Phonon softening and crystallographic orientation of strained graphene studied by Raman spectroscopy.," *Proc. Natl. Acad. Sci. U. S. A.*, vol. 106, no. 18, pp. 7304–8, May 2009.

[44] T. M. G. Mohiuddin *et al.*, "Uniaxial strain in graphene by Raman spectroscopy: G peak splitting, Grüneisen parameters, and sample orientation," *Phys. Rev. B*, vol. 79, no. 20, p. 205433, May 2009.

[45] A. C. Ferrari, S. E. Rodil, and J. Robertson, "Resonant Raman spectra of amorphous carbon nitrides: The G peak dispersion," *Diam. Relat. Mater.*, vol. 12, no. 3–7, pp. 905–910, Mar. 2003.

[46] M. S. Dresselhaus, A. Jorio, A. G. Souza Filho, and R. Saito, "Defect characterization in graphene and carbon nanotubes using Raman spectroscopy," *Philos. Trans. R. Soc. A Math. Phys. Eng. Sci.*, vol. 368, no. 1932, pp. 5355–5377, 2010.

[47] C. Casiraghi *et al.*, "Raman spectroscopy of graphene edges," *Nano Lett.*, vol. 9, no. 4, pp. 1433–1441, Apr. 2009.

[48] R. Saito, "Raman spectroscopy of graphene edges," in *Graphene and its Fascinating Attributes*, vol. 9, no. 4, American Chemical Society, 2011, pp. 91–103.

[49] D. Bischoff, J. Güttinger, S. Dröscher, T. Ihn, K. Ensslin, and C. Stampfer, "Raman spectroscopy on etched graphene nanoribbons," *J. Appl. Phys.*, vol. 109, no. 7, p. 073710, May 2011.

[50] F. Tuinstra, J. L. Koenig, and L. Koenig, "Raman Spectrum of Graphite," *J. Chem. Phys.*, vol. 53, no. 1970, pp. 1126–1130, Aug. 1970.

[51] M. M. Lucchese *et al.*, "Quantifying ion-induced defects and Raman relaxation length in graphene," *Carbon*, vol. 48, no. 5, pp. 1592–1597, 2010.

[52] A. C. Ferrari, “Raman spectroscopy of graphene and graphite: Disorder, electron-phonon coupling, doping and nonadiabatic effects,” *Solid State Commun.*, vol. 143, no. 1–2, pp. 47–57, 2007.

[53] L. M. Malard *et al.*, “Probing the electronic structure of bilayer graphene by Raman scattering,” *Phys. Rev. B - Condens. Matter Mater. Phys.*, vol. 76, no. 20, Aug. 2007.

[54] Y. Hao *et al.*, “Probing layer number and stacking order of few-layer graphene by Raman Spectroscopy,” *Small*, vol. 6, no. 2, pp. 195–200, 2010.

[55] D. Kostiuk *et al.*, “Reliable determination of the few-layer graphene oxide thickness using Raman spectroscopy,” *J. Raman Spectrosc.*, vol. 47, no. 4, pp. 391–394, 2016.

[56] S. Roscher, R. Hoffmann, and O. Ambacher, “Determination of the graphene-graphite ratio of graphene powder by Raman 2D band symmetry analysis,” *Anal. Methods*, vol. 11, no. 9, pp. 1180–1191, Feb. 2019.

[57] A. C. Ferrari and J. Robertson, “Raman Spectroscopy of Amorphous, Nanostructured, Diamond-like Carbon, and Nanodiamond,” *Philosophical Transactions: Mathematical, Physical and Engineering Sciences*, vol. 362. Royal Society, pp. 2477–2512.

[58] R. Saito, “Raman spectroscopy of graphene edges,” *Graphene its Fascin. Attrib.*, vol. 9, no. 4, pp. 91–103, Apr. 2011.

[59] Z. P. LUO and J. H. KOO, “Quantifying the dispersion of mixture microstructures,” *J. Microsc.*, vol. 225, no. 2, pp. 118–125, Feb. 2007.

[60] J. Zhang, H. Yang, G. Shen, P. Cheng, J. Zhang, and S. Guo, “Reduction of graphene oxide vial-ascorbic acid,” *Chem. Commun.*, vol. 46, no. 7, pp. 1112–1114, 2010.

[61] Z. Shen, J. Li, M. Yi, X. Zhang, and S. Ma, “Preparation of graphene by jet cavitation,” *Nanotechnology*, vol. 22, no. 36, p. 365306, 2011.